

# Topological data analysis reveals differences between simulated galaxies and dark matter haloes

Aaron Ouellette,<sup>1,2</sup>★ Gilbert Holder,<sup>1</sup> Ely Kerman<sup>3</sup>

<sup>1</sup>*Department of Physics, University of Illinois at Urbana-Champaign, Urbana, IL 61801, USA*

<sup>2</sup>*Center for AstroPhysical Surveys, National Center for Supercomputing Applications, Urbana, IL 61801, USA*

<sup>3</sup>*Department of Mathematics, University of Illinois at Urbana-Champaign, Urbana, IL 61801, USA*

Accepted XXX. Received YYY; in original form ZZZ

## ABSTRACT

We use topological summaries based on Betti curves to characterize the large-scale spatial distribution of simulated dark matter haloes and galaxies. Using the IllustrisTNG and CAMELS-SAM simulations, we show that the topology of the galaxy distribution is significantly different from the topology of the dark matter halo distribution. Further, there are significant differences between the distributions of star-forming and quiescent galaxies. These topological differences are broadly consistent across all simulations, while at the same time there are noticeable differences when comparing between different models. Finally, using the CAMELS-SAM simulations, we show that the topology of the quiescent galaxies, in particular, depends strongly on the amount of supernova feedback. These results suggest that topological summary statistics could be used to help better understand the processes of galaxy formation and evolution.

**Key words:** large-scale structure of Universe – galaxies: haloes – galaxies: formation – methods: data analysis

## 1 INTRODUCTION

One of the biggest challenges in cosmology today is understanding the effects of galaxy formation and evolution on the distribution of matter in the universe (van Daalen et al. 2011; Chisari et al. 2019). Many upcoming observational programs, such as DESI (DESI Collaboration et al. 2016), LSST (Ivezić et al. 2019), Euclid (Laureijs et al. 2011), CMB-S4 (Abazajian et al. 2019), and others, are poised to collect vast amounts of data that will help further constrain cosmological models, but robust models of baryonic effects are necessary in order to ensure that statistical uncertainties are not overwhelmed by systematic ones.

On the theory side, large cosmological simulations aim to simulate the formation and evolution of galaxies and the growth of large-scale structure from first principles. It is now well established through cosmological hydrodynamic simulations such as EAGLE (Schaye et al. 2015; Crain et al. 2015), Illustris (Nelson et al. 2015; Vogelsberger et al. 2014), and IllustrisTNG (Nelson et al. 2019) that feedback from active galactic nuclei (AGN) and supernovae is vital to produce realistic galaxies. However, these simulations all have very different implementations of feedback models, leaving some uncertainty in their specific predictions. Consequently, it is necessary to develop statistical probes that are best suited to constrain these models.

The usual statistical probe of large-scale structure is the 2-point correlation function, or its Fourier transform, the power spectrum. This is the ideal summary statistic in the case of Gaussian random fields, which are fully described by their 2-point functions, but cosmological density fields are non-Gaussian. An increasing amount of literature suggests that probes that encode information about the

higher-order moments of clustering beyond the 2-point correlation function are extremely useful in providing cosmological constraints. In addition to the higher  $n$ -point functions, these include counts-in-cells (Peebles 1980; Leicht et al. 2019; Uhlemann et al. 2020; Perez et al. 2022), void probability functions (White 1979; Conroy et al. 2005; Perez et al. 2021), nearest neighbor distributions (Banerjee & Abel 2021), network statistics (Coutinho et al. 2016; Hong et al. 2016; Naidoo et al. 2020), and many others. These probes generally have the advantage that they are relatively easy to compute, and they include information from higher-order clustering. On the other hand, they are usually much harder to predict directly from theory compared to the power spectrum or 2-point function.

It is now well known that on large scales, the distribution of matter in the universe forms a highly complex and connected structure known as the cosmic web (Bond et al. 1996; van de Weygaert & Bond 2008; Libeskind et al. 2018). This structure naturally lends itself to description through the ideas of topology. The topology of the cosmic web has been studied since the advent of large redshift surveys (Gott et al. 1986; Hamilton et al. 1986; Weinberg et al. 1987; Gott et al. 1987, 1989; Melott et al. 1988, 1989). Recent advances in the fields of computational topology and topological data analysis (TDA) have provided principled and efficient methods for statistically describing the "shape of data." This is often done using a formalism called persistent homology, where one characterizes the topological features present in data as a function of scale. An overview can be found in Carlsson (2009).

These methods from TDA have just recently started to see applications in cosmology and astrophysics, but the breadth of applications has been quite wide. van de Weygaert et al. (2010, 2011) proposed using persistent homology and Betti numbers to characterize the large-scale structure of the cosmic web and Sousbie (2011) used

★ E-mail: aaronjo2@illinois.edu

ideas from topology to develop a robust method of identifying clusters, filaments, and voids in the cosmic web. Studies on dark matter (DM) haloes and the cosmic web were done by [Pranav et al. \(2017\)](#); [Bermejo et al. \(2022\)](#); [Tsizh et al. \(2023\)](#). Other applications include [Xu et al. \(2019\)](#), who developed a formalism to identify statistically significant voids and filaments. [Kono et al. \(2020\)](#) used persistent homology to identify the baryon acoustic oscillation features in the spatial distribution of galaxies. [Cisewski-Kehe et al. \(2022\)](#) showed that TDA is able to discriminate between different DM models using only subhalo spatial distributions. Persistent homology has also been applied to study the period of re-ionization ([Elbers & van de Weygaert 2019, 2023](#); [Th  lie et al. 2022](#)), the analysis of weak lensing data ([Heydenreich et al. 2021, 2022](#)), and to detect signatures of non-Gaussianity in the primordial density fluctuations [Cole et al. \(2020\)](#); [Biagetti et al. \(2021, 2022\)](#). Most similar to our work is that of [Bermejo et al. \(2022\)](#), where the authors explored the topology of DM haloes using persistent homology. They reported a “topological bias”: haloes exhibited different topologies that depended on mass.

In this work, we use Betti curves from persistent homology to characterize the large-scale structure of galaxies and DM haloes, taking into account the potentially confounding effects of number density. We then show that these topological summaries reveal differences in the large-scale structure of haloes and different galaxy populations. Our main results are as follows. First, we find that DM haloes exhibit a nearly universal topology across a wide range of scales. While haloes selected by mass cluster very differently, after taking into account their number density, we find that topologically they are in fact very similar. Galaxies, on the other hand, exhibit surprising differences on small scales. We find that a second physical scale shows up in the topology of galaxies that is not present in the haloes. Further, separating galaxies into star-forming and quiescent sub-samples reveals that the topology of quiescent galaxies is especially sensitive to differences in the feedback model used. Based on these results, we argue that galaxies are topologically distinct from DM haloes and that topological summaries could provide very useful information in order to better constrain models of galaxy formation and evolution.

This paper is structured as follows. In [section 2](#) we review the basics of topological data analysis. Our analysis pipeline is outlined in [section 3](#). Next we calibrate our method in [section 4](#) by exploring the topology of samples of random points. We introduce the simulations and mock galaxy catalogs used in this work in [section 5](#). In [section 6](#) we present our main results. We conclude in [section 7](#).

## 2 OVERVIEW OF TOPOLOGICAL DATA ANALYSIS

Topology in the traditional sense is concerned with properties of manifolds that are invariant under continuous deformations. One of the most intuitively familiar formulations of topology is *homology* – the characterization of “holes” in a topological space. Formally, this is described through homology groups, the rank of which represents the number of independent topological features. The full formal mathematical description of homology is beyond the scope of this work, but is laid out in many textbooks on algebraic topology, such as [Hatcher \(2001\)](#). More details on the computational aspects of topology can be found in [Edelsbrunner & Harer \(2010\)](#). Here, we will focus on providing an intuitive summary that will be useful for understanding applications of topology to cosmological datasets.

In three dimensional space, there are three possible types of “holes”, characterized by their dimension:  $H_0$ ,  $H_1$ , and  $H_2$ .  $H_0$  represents connected components of the space,  $H_1$  represents classes of loops enclosing independent tunnels, and  $H_2$  represents classes

of shells enclosing independent voids. *Betti numbers*  $\beta_d$  can then be defined for each dimension as simply the count of independent features (formally,  $H_d$  is a group, the rank of which is  $\beta_d$ ). As a simple example, a two-sphere has Betti numbers  $\beta_0 = 1$ ,  $\beta_1 = 0$ ,  $\beta_2 = 1$  (one connected component, zero non-contractible loops, and one enclosed void), while a two-torus has Betti numbers  $\beta_0 = 1$ ,  $\beta_1 = 2$ ,  $\beta_2 = 1$  (in the torus there are two independent classes of loops).

### 2.1 Persistent homology

Persistent homology ([Edelsbrunner et al. 2002](#); [Carlsson et al. 2005](#); [Ghrist 2007](#)) is a formalism to quantify the homology of a topological space as a function of scale. This turns out to be ideal in a cosmological setting since the properties of the matter distribution are very much scale dependent: at very large scales the universe looks homogeneous and isotropic, at intermediate scales we get the filamentary cosmic web, and at small scales we might see individual clusters of galaxies.

Here, we focus on the application of persistent homology to data in the form of a point cloud<sup>1</sup> (e.g., galaxy catalogs). In order to compute topological quantities, we need some way of transforming the disconnected points into a topological space that in some way captures the “shape” of the underlying data. This is often done using *simplicial complexes* which can be thought of as a triangulation of the topological space represented by the point set. Formally, a  $k$ -simplex is the convex hull of  $k + 1$  affinely independent points. Simply, this means that in three dimensions, there are 4 possible simplices: a point (vertex), a line segment (edge), a triangle, and a tetrahedron. These simplices can be connected together to build a simplicial complex. Simplicial complexes then allow for easy combinatorial descriptions of topological spaces and provide for a standard way to compute homology.

Simplicial complexes can be associated to a point cloud at different scales, leading to a nested family of complexes called a *filtration*. One of the commonly used filtrations is the Vietoris-Rips filtration whose scaling parameter is defined in terms of the pairwise distances between points in the dataset. The simplicial complex of the Vietoris-Rips filtration at scale  $r$  is comprised of the points in the given point cloud together with all the higher dimensional simplices whose vertices are all within a distance  $r$  from one another.

For large datasets, Vietoris-Rips filtrations become prohibitively expensive to compute, since calculating pairwise distances scales quadratically with the number of points. For this reason, we use a filtration based on alpha complexes ([Edelsbrunner et al. 1983](#); [Edelsbrunner & M  cke 1994](#)), which are subcomplexes of the Delaunay triangulation. The alpha complex filtration is parameterized by the filtration parameter  $\alpha$ . At  $\alpha = 0$ , the alpha complex consists only of the vertices in the point cloud. As  $\alpha$  increases, simplices from the Delaunay triangulation are added to the complex if they are contained inside a closed ball of radius less than  $\alpha$  that has no vertices in its interior, or they are in the boundary of 3-simplices or 2-simplices that meet these criteria. Construction of the alpha complex has sub-quadratic scaling with the number of points. (The construction scales exponentially with the number of dimensions, but our data is all three dimensional.)

Once we have chosen a filtration, it is fairly straightforward to compute the homology of the resulting simplicial complexes as a

<sup>1</sup> Persistent homology can also be applied to data in the form of scalar fields, such as density fields, as is done in [Pranav et al. \(2019\)](#); [Pranav \(2021\)](#).

function of scale (represented by the filtration parameter). As the filtration parameter  $\alpha$  grows, a homology class may appear at some value  $\alpha_{\text{birth}}$ , persist for some range, and then may disappear at some larger value  $\alpha_{\text{death}}$  (this will be illustrated in more detail in Figure 1, see section 3). These pairs of births and deaths are tracked in a *persistence diagram* in which each is represented by its corresponding interval,  $[\alpha_{\text{birth}}, \alpha_{\text{death}}]$ . The persistence diagram will also contain one infinitely long interval of the form  $[\alpha_{\text{birth}}, \infty)$  for each nontrivial homology class of the ambient space in which the data lives. For example, in Euclidean space, there will be a single infinite interval in the  $H_0$  persistence diagram, representing the fact that at a certain scale all points in the dataset will become connected.

## 2.2 Topological summaries

Persistence diagrams provide useful summaries of the topological features in a dataset, but they are not convenient to work with statistically. While measures of differences between two diagrams exist (e.g. the bottleneck distance or  $p$ -Wasserstein distance), they are very computationally intensive since some optimal matching between points in different diagrams is necessary. Additionally, a mean can be defined on the space of persistence diagrams (Turner et al. 2014), but it is not necessarily unique and suffers from the same computational challenges.

The standard way of solving this problem is to define a functional summary of persistence diagrams (Berry et al. 2020). This is a mapping from the space of persistence diagrams to the space of functions of the filtration parameter that encodes in some way the information present in a persistence diagram. There are many ways to do this that have been defined in the TDA literature, some common examples are: Betti curves, landscape functions (Bubenik 2012), weighted silhouettes (Chazal et al. 2013), and entropy summary functions (Atienza et al. 2020). Each of these functional summaries has different trade-offs between interpretability, robustness to noise, and the amount of information retained from the persistence diagram.

In this work, we focus on Betti curves, since they are perhaps the simplest and most interpretable summary available. A Betti curve is a direct generalization of Betti numbers: for a given homology dimension  $d$ ,  $\beta_d(\alpha)$  is simply the  $d^{\text{th}}$  Betti number of the simplicial complex at the corresponding value of the filtration parameter.

## 3 ANALYSIS PIPELINE

In general, the analysis pipeline to apply TDA to point cloud data consists of the following steps.

- (i) Define a simplicial complex on the point cloud that depends on a filtration parameter.
- (ii) For each value of the filtration parameter, calculate the homology of the resulting complex.
- (iii) Track the birth and death scales of the homology features in a persistence diagram.
- (iv) Calculate a functional summary of the persistence diagram in order to statistically quantify the topology.

In this work, the data consists of galaxy (or halo) positions. These galaxies and haloes come from cosmological simulations that use periodic boundary conditions, hence our data and alpha complexes naturally live in the three dimensional torus instead of  $\mathbb{R}^3$ . We exclude the topology of the ambient torus, leaving only the topology of the galaxy and halo distributions, by deleting all infinitely long intervals in our persistence diagrams. The resulting persistence diagrams are

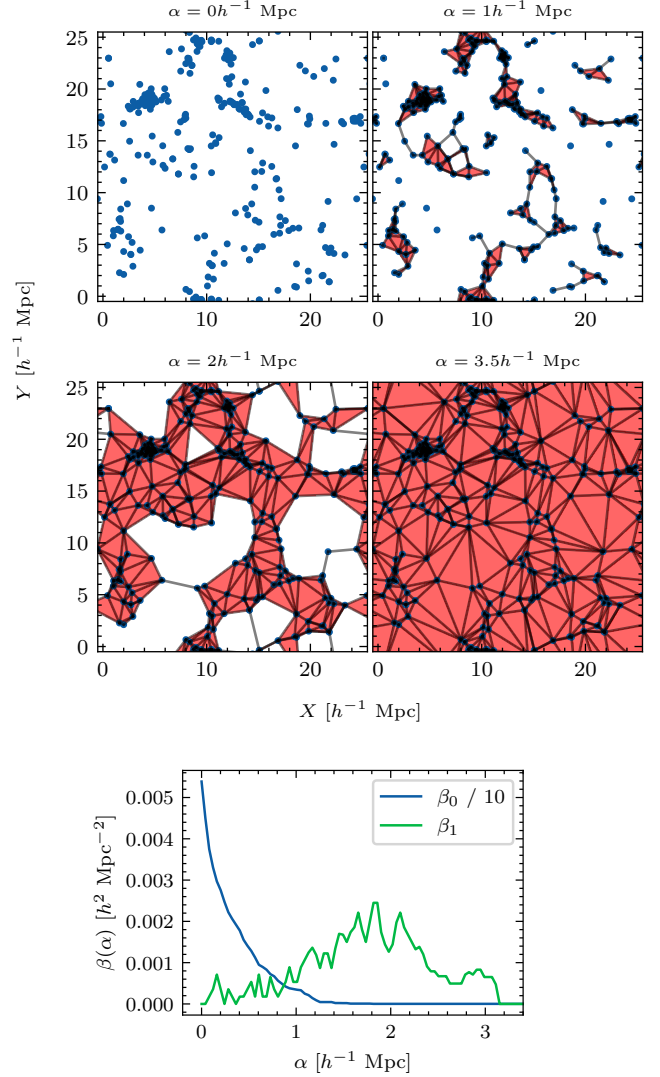


**Figure 1.** *Top:* Two-dimensional Visualization of the evolution of the alpha complex for a slice of galaxies. Here we took galaxies in a 6 Mpc slice from the EX0 simulation of the CAMELS IllustrisTNG suite. The panels show the resulting alpha complexes for increasing values of  $\alpha$ . *Bottom:* Betti curves, showing the full evolution of the number of homology features as a function of scale. Note that the Betti curves are given per unit area since this example is set in 2D.

then used to compute Betti curves that track the number of homology features as a function of scale. We report Betti numbers normalized by volume, i.e., the number density of various homology features.

We use a Python wrapper<sup>2</sup> around the C++ library GUDHI<sup>3</sup> (The GUDHI Project 2022) to construct periodic alpha complexes and compute their persistent homology. Betti curves and other summary functions are implemented in the representations module of the GUDHI Python package (Dlotko 2022).

To provide a concrete example of this process, in Figure 1 we show how an alpha complex filtration is constructed for a small set of galaxies from a cosmological simulation. We selected galaxies in a  $6h^{-1}$  Mpc thick slice from the EX0 simulation of the CAMELS

<sup>2</sup> <https://github.com/ajouellette/alpha-complex-wrapper>

<sup>3</sup> <https://gudhi.inria.fr>

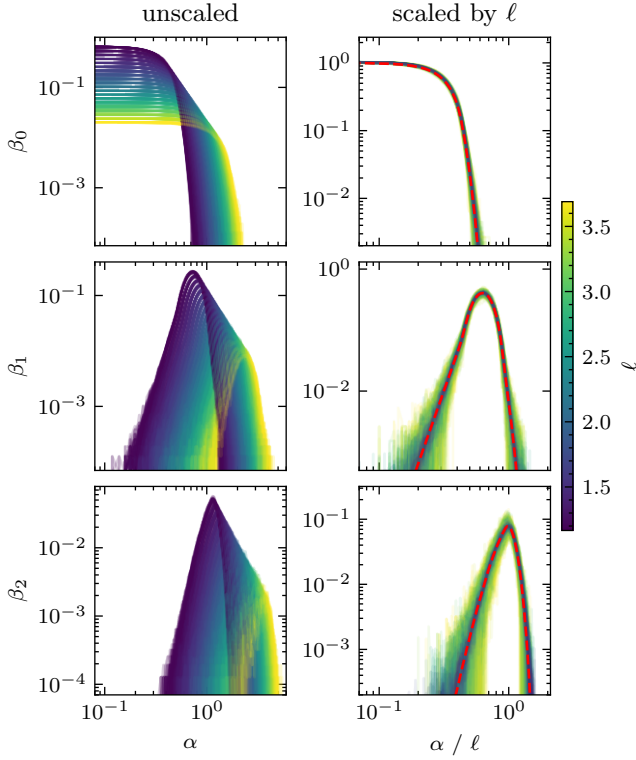


**Figure 2.** Betti curves for Poisson point processes. *Left column:* 0-, 1-, and 2-dim Betti curves for 1,000 different samples of uniformly distributed points with  $L = 25$ . The colors indicate the mean particle separation  $\ell = L/N^{1/3}$  for each sample of random points.  $\alpha$  has arbitrary units of length and the Betti curves have arbitrary units of inverse volume. *Right column:* scaled Betti curves for the same 1,000 random point samples. The dashed red line indicates the average scaled Betti curve for a larger box with  $L = 75$ .

IllustrisTNG suite<sup>4</sup>. For visualization purposes, this example is set in 2D. The top 4 panels in Figure 1 show the resulting alpha complexes for given values of the filtration parameter  $\alpha$ . As we increase  $\alpha$ , the number of disconnected components (or separate clusters of points) decreases rapidly while loops gradually form and then disappear at larger values of  $\alpha$ . Finally, at a scale of  $3.5h^{-1}$  Mpc, only one large connected component remains. If we track this evolution for all values of  $\alpha$ , we can compute the Betti curves (normalized by the area of the 2D box) for homology dimensions 0 and 1. These are shown in the bottom panel of Figure 1, where we see the rapid decrease in the number of disconnected components ( $\beta_0$ ) and a rise and then fall in the number of loops ( $\beta_1$ ).

#### 4 TOPOLOGY OF RANDOM POINTS

In order to rigorously compare the topologies of different galaxy samples, we first explore how the topology depends on the properties of various random point processes. Specifically, we look at uniformly distributed points and points sampled from log-normal fields. In both cases, the points are sampled inside a 3D periodic box of size  $L$ .

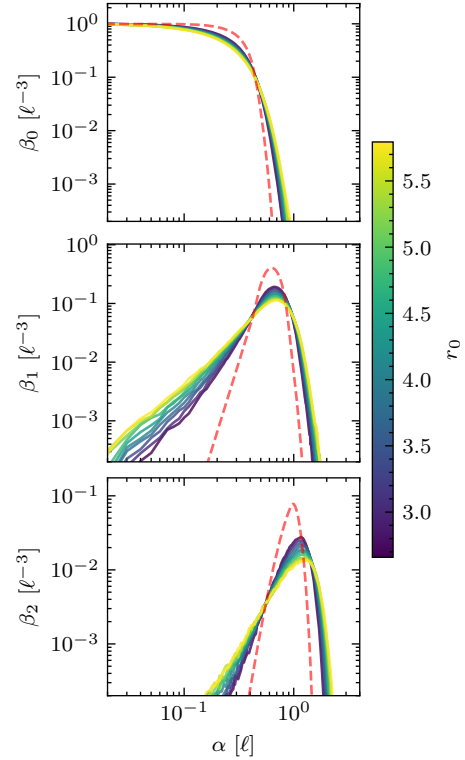


**Figure 3.** Scaled Betti curves for log-normal point processes following a power-law correlation function. The mean Betti curves for a Poisson point process are overlaid with the red dashed line.

#### 4.1 Uniformly distributed points

First, we consider the simplest case – random points uniformly distributed inside a cube with sides  $[0, L)$  (i.e., a Poisson point process). In this case, the points are characterized only by the average number density  $n = N/L^3$  or mean separation  $\ell = 1/n^{1/3}$ . Since the persistent homology of a point cloud directly depends on the pairwise distances between the points, we expect the topological summaries to be strongly dependent on  $\ell$ , especially in the case where this is the only characteristic length of the point sample.

To test this, we generated 1,000 samples of random points uniformly distributed in a 3D periodic box of size  $L = 25$  with a wide range of values for  $\ell$ . For each collection of points, we computed their persistent homology using periodic alpha complexes and calculated Betti curves for each of the 3 homology dimensions. The results are shown in the left column of Figure 2. We see a strong dependence on  $\ell$ , however the curves for a given dimension generally have the same shape.

We would like a topological summary that does not depend on the number density of points, but rather captures the intrinsic shape of the data. In this very simple case of uniformly distributed points, the solution is very simple. All point samples should become self-similar if we scale all distances by  $\ell$ . Applying this to the Betti curves, we scale the filtration parameter by  $\ell$  and re-normalize the Betti curves by a volume of  $\ell^3$ . The results are shown in the right column of Figure 2. We see that the scaled curves are now roughly identical; the outliers tend to be the point samples with the fewest points (corresponding to larger statistical noise). These curves now show a summary of the universal topology of samples from Poisson point processes. Additionally, we confirm that this topological summary does not depend significantly on the box size. We applied the same method

<sup>4</sup> <https://camels.readthedocs.io/en/latest/>



to 1,000 realizations inside a larger box with  $L = 75$  and calculated the average Betti curve for each homology dimension. These curves are shown in the same figure with the red dashed lines and match the previous curves very well.

We note that similar results can be found in the math literature in relation to percolation theory or the theory of random graphs (Robins 2002, 2006, for example).

## 4.2 Log-Normal fields

Galaxy samples are obviously not well represented by uniformly distributed random points. Next, we explore how clustering affects the topological summary functions.

To mimic the clustering of galaxies, we generate log-normal fields (suggested as a model for galaxy distributions by Coles & Jones 1991) with a power-law power spectrum. In real space, this results in a 2-point correlation function that can be written as

$$\xi(r) = \left(\frac{r}{r_0}\right)^\gamma. \quad (1)$$

We use the Python package `powerbox`<sup>5</sup> (Murray 2018) to generate 500 samples from log-normal fields with power-law clustering using a fixed exponent of  $\gamma = -1.5 \pm 0.1$  and a wide range of values for the clustering length  $r_0$ . As before, for each sample we calculate its persistent homology and convert the persistence diagrams into scaled Betti curves. To reduce statistical noise, we also bin the samples by their clustering length and average the corresponding Betti curves.

In Figure 3, we plot the averaged scaled Betti curves for 8 bins between  $r_0 = 3$  and  $r_0 = 6$ , with the mean scaled Betti curves for a Poisson point process overlaid. We see that, compared to the number density, the clustering of points is a small effect, causing slight shifts in the Betti curves. Increasing the clustering length suppresses the peak of the  $H_1$  and  $H_2$  Betti curves and lengthens the tails.

## 5 COSMOLOGICAL SIMULATIONS

We use galaxy and halo catalogs derived from two simulation suites: IllustrisTNG<sup>6</sup> and CAMELS-SAM<sup>7</sup>. We chose these simulations in order to compare roughly similar models at a large enough size (box sizes of at least  $\sim 100h^{-1}$  Mpc) so that the results are less affected by sample variance.

The IllustrisTNG simulations (Springel et al. 2018; Nelson et al. 2018; Pillepich et al. 2018; Marinacci et al. 2018; Naiman et al. 2018) are large high-resolution cosmological magnetohydrodynamic simulations that aim to fully model the galaxy formation process in a cosmological context. Here we use publicly released data from the TNG300 run (Nelson et al. 2019). The TNG simulations were run using the AREPO code (Weinberger et al. 2020). TNG300 uses a simulation box of comoving size  $L = 205 h^{-1}$  Mpc and tracks the evolution of  $2 \times 2500^3$  DM particles and gas cells. The simulation assumes a standard flat  $\Lambda$ CDM universe with  $\Omega_m = 0.3089$ ,  $\Omega_b = 0.0486$ ,  $\sigma_8 = 0.8159$ ,  $n_s = 0.9667$ , and  $h = 0.6774$ . Additionally, a complex supernova and AGN feedback model is used to model realistic galaxy formation (Weinberger et al. 2017; Pillepich et al. 2018). The halo and galaxy catalogs for the TNG simulations were generated by running SUBFIND (Springel et al. 2001).

The CAMELS-SAM simulation set is a large suite of simulated galaxies that specifically aims to test the effects of wide ranges of both cosmological and astrophysical parameters (Perez et al. 2022; Villaescusa-Navarro et al. 2022). CAMELS-SAM is based on 1,005 DM-only simulations inside a box with  $L = 100h^{-1}$  Mpc, tracking the evolution of  $N = 640^3$  particles using AREPO. These simulations cover a broad space of cosmological models by varying  $\Omega_m$  (between 0.1 and 0.5) and  $\sigma_8$  (between 0.6 and 1.0), but otherwise assume a standard flat  $\Lambda$ CDM model with  $\Omega_b = 0.049$ ,  $h = 0.6711$ , and  $n_s = 0.9624$ . Halo catalogs and merger trees were generated using Rockstar (Behroozi et al. 2013a) and ConsistentTrees (Behroozi et al. 2013b). Galaxy catalogs were generated by running multiple iterations of the Santa Cruz semi-analytic (SC-SAM) model of galaxy formation (Somerville & Primack 1999; Somerville et al. 2008, 2015), varying the amount of supernova and AGN feedback. The feedback in the SC-SAM model is varied in these simulations through three normalization parameters:  $A_{SN1}$ ,  $A_{SN2}$ , and  $A_{AGN}$ .

The CAMELS-SAM simulations are further divided into 3 subsets: CV (cosmic variance), 1P (one parameter), and LH (latin hypercube). The CV set consists of 5 simulations using the fiducial model ( $\Omega_m = 0.3$ ,  $\sigma_8 = 0.8$ ,  $A_{SN1} = 1$ ,  $A_{SN2} = 0$ , and  $A_{AGN} = 1$ ), but with random initial seeds in order to quantify the amount of sample variance. The 1P set consists of 12 simulations that vary the three astrophysical parameters one at a time, keeping all other parameters at their fiducial values. Finally, the LH set consists of 1,000 simulations that simultaneously vary all 5 parameters and the initial seed.

Ideally, we would have also used the full hydrodynamic simulations from the CAMELS suite, but the box sizes of  $25h^{-1}$  Mpc were too small for our purposes. Each simulation box has on average only  $\sim 800$  galaxies, making sub-selections based on various properties not viable. Additionally, sample variance due to the small box size overwhelmed variances due to parameter variations.

## 6 RESULTS

Here we present three main results. (1) DM haloes exhibit a nearly universal topology, independent of mass. (2) Galaxies are topologically different from the haloes on small scales. (3) The topology of quiescent galaxies is significantly different from that of the star-forming ones and is especially sensitive to the feedback model used.

### 6.1 DM haloes

In this section, we quantify the topology of the DM halo distribution in order to make comparisons with galaxies in the next sections. Here we focus on the TNG300 simulation due to its large size. We define haloes using a spherical overdensity of 200 times the critical density of the universe, thus all halo masses given refer to  $M_{200c}$ . We consider haloes above a minimum mass cut of  $M_{200c} > 3.2 \times 10^{10} h^{-1} M_\odot$ , very roughly corresponding to at least 450 simulation particles in each halo. There are a total of  $5.37 \times 10^5$  such haloes in TNG300, allowing us to further divide them into several mass bins to look at the dependence of topology on halo mass.

We divide our total halo sample into four mass bins, based on the value of  $\log_{10}(M_{200c} [h^{-1} M_\odot])$ : 10.5 to 11, 11 to 11.5, 11.5 to 12, and above 12. For each halo sample, we calculate its 2-point correlation function  $\xi(r)$  using the Landy-Szalay estimator (Landy & Szalay 1993) implemented in `Corrfunc`<sup>8</sup> (Sinha et al. 2021). We then

<sup>5</sup> <https://github.com/steven-murray/powerbox>

<sup>6</sup> <https://www.tng-project.org/>

<sup>7</sup> <https://camels-sam.readthedocs.io/en/main/>

<sup>8</sup> <https://github.com/manodeep/Corrfunc>

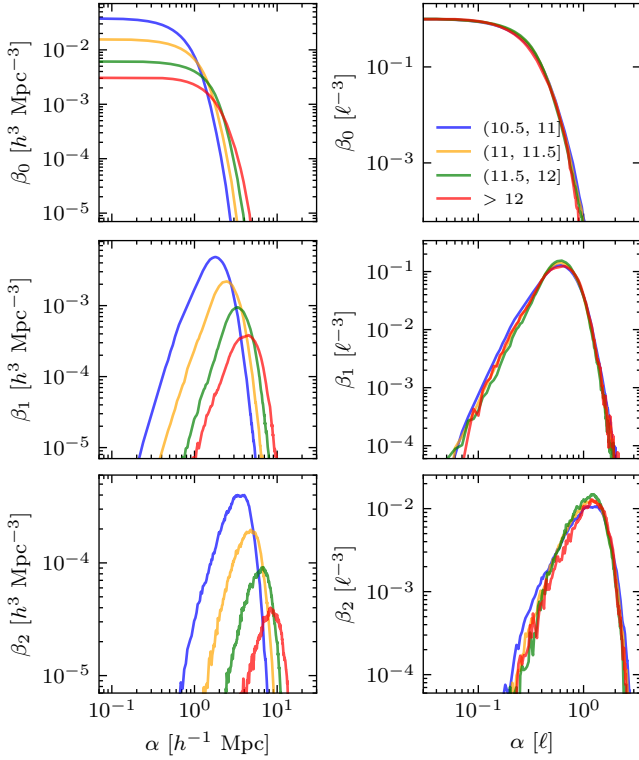


**Figure 4.** Betti curves for TNG300 haloes in four different mass bins. *Left:* unscaled Betti curves. The curves appear to be self-similar with roughly the same shape, but vastly different physical scales. *Right:* scaled Betti curves. Haloes of all masses show a nearly universal topology.

$\log(M_{200c}/M_{\odot})$	$N_{\text{haloes}}$	$\ell$ [ $h^{-1}$ Mpc]	$r_0$ [ $h^{-1}$ Mpc]	$\gamma$
(10.5, 11]	$3.2 \times 10^5$	2.99	2.29	-1.41
(11, 11.5]	$1.3 \times 10^5$	4.01	2.53	-1.45
(11.5, 12]	$5.3 \times 10^4$	5.47	3.00	-1.50
> 12	$2.6 \times 10^4$	6.89	4.21	-1.52

**Table 1.** Summary of the TNG300 DM haloes divided into four mass bins to compare their topologies. We list the number of haloes in each bin, the mean particle separation, and the parameters used to fit a power law to the correlation functions.

fit a power-law (Equation 1) to each halo sample in order to estimate each sample’s clustering length  $r_0$ . Additionally, we calculate the mean separation  $\ell = L/N^{1/3}$  for each sample. The properties of each halo sample are summarized in Table 1. As expected, we see that higher mass haloes are much rarer and more clustered than lower mass haloes. Clearly, the 2-point correlation function easily differentiates these halo samples, but we would like to test whether these samples are different topologically.

We construct periodic alpha-complex filtrations for each halo sample and compute the corresponding Betti curves (ignoring the persistence pairs at infinity as mentioned in section 3). In the left column of Figure 4, we plot the unscaled Betti curves normalized by the volume of the simulation box. In these panels, we see that the Betti curves across the different samples have roughly the same shape, but lie at vastly different scales. As seen in section 4, this is due to the vastly different number of haloes in each sample: fewer haloes will directly lead to fewer loops or voids present, and those present will occur at larger physical scales. The presence of different clustering

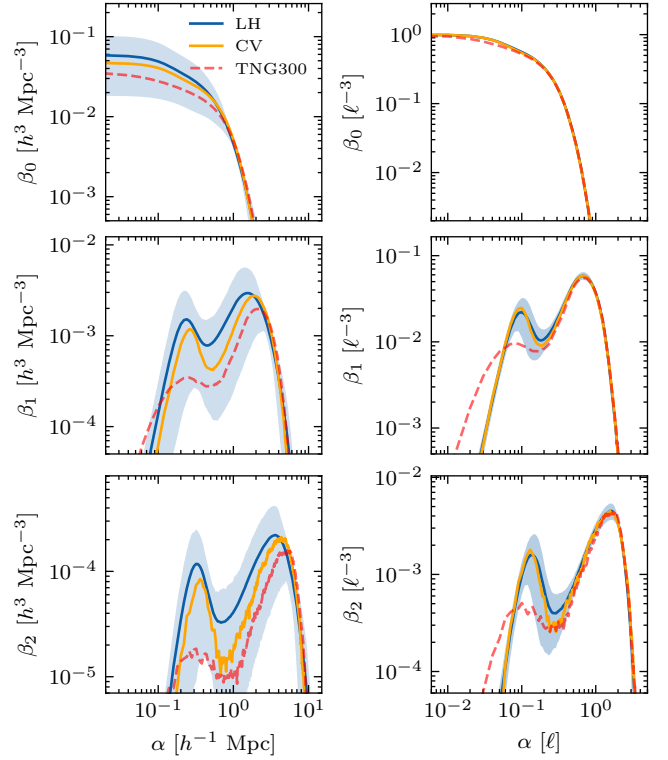


**Figure 5.** Betti curves for all galaxies in the CAMELS-SAM and TNG300 catalogs. The bands around the CAMELS-SAM curves indicate roughly  $1\sigma$  variation around the mean. *Left:* unscaled Betti curves. *Right:* scaled Betti curves.

lengths  $r_0$  also complicates things, but this is a second-order effect. We must first scale out the dependence on the number density of haloes.

The right column of Figure 4 shows the same Betti curves for the TNG300 haloes, but now re-scaled by  $\ell$  and re-normalized to represent the number of homology features within a cube of size  $\ell$ . The scaled Betti curves look almost identical, indicating that all four samples of DM haloes exhibit the same underlying topology.

In contrast, Bermejo et al. (2022) scaled the Betti curves by the clustering length  $r_0$  instead of the mean separation  $\ell$  and found residual differences in topology. However, we find that differences between halo mass bins are largely driven by number density. Topological summaries in terms of  $\ell$  show a topology that is independent of resolution.

Additionally, we note that these Betti curves look distinct from those of the log-normal fields with similar clustering. This shows that Betti curves are indeed sensitive to higher moments of clustering.

## 6.2 Galaxies

Next, we look at galaxies and various sub-selections of galaxies. We use both CAMELS-SAM and TNG300 in order to compare two different models of galaxy formation. In the TNG300 simulation, we select all subhaloes with at least a 10% DM mass fraction. As noted in Springel et al. (2018), this filters out a small population of baryonic lumps, most likely produced by disk fragmentation. The CAMELS-SAM catalogs already only include galaxies due to the SC-SAM directly modelling galaxy formation inside the DM haloes. For both simulations, we additionally impose a minimum stellar mass cut of

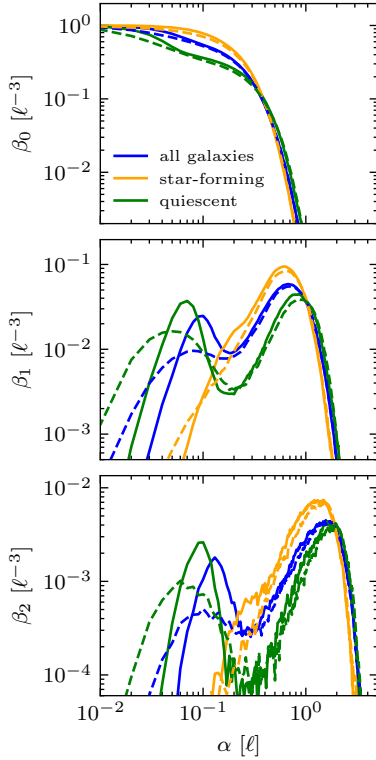


**Figure 6.** Scaled Betti curves for different galaxy subsets. Here the color of the curve indicates the type of galaxy considered (all galaxies, star-forming, or quiescent), solid lines indicate the CAMELS-SAM fiducial model, and dashed lines indicate the TNG300 model. The bands around the CAMELS-SAM curves indicate  $2\sigma$  variance around the mean.

$5 \times 10^8 h^{-1} M_\odot$ . We further divide both galaxy samples into star-forming and quiescent galaxies. Following [Humphrey et al. \(2022\)](#), we define the boundary between star-forming and quiescent to be a specific star formation rate (sSFR) of  $10^{-10.5} \text{ yr}^{-1} = 0.0316 \text{ Gyr}^{-1}$ .

[Figure 5](#) shows the Betti curves for all of the galaxies from the CAMELS-SAM and TNG300 samples. We immediately see that these Betti curves are significantly different than those for the DM haloes. Both the  $H_1$  and the  $H_2$  Betti curves have a second peak at small scales that was not present in the halo Betti curves or the random samples in [section 4](#). This indicates that galaxies have additional structure on small scales that is not present in the haloes. In the unscaled Betti curves this second peak occurs roughly at a scale of  $200 h^{-1} \text{ kpc}$ , possibly due to small-scale structures in galaxy clusters. Additionally, the Betti curves for the TNG300 and SC-SAM models are significantly different at small scales, due to inherent differences in the galaxy formation models.

[Figure 6](#) shows the scaled Betti curves for all three samples of galaxies (all, star-forming, quiescent) for both TNG300 and the fiducial CAMELS-SAM model. Here we see that there are significant differences between the Betti curves of quiescent and star-forming galaxies. The peak at small scales only appears in the curves for the quiescent galaxies. This supports our speculation that the small scale peak is due to galaxy clusters, as galaxies in large clusters tend to be quiescent (see, for example, [Peng et al. 2010](#); [Wetzel et al. 2013](#)).

### 6.3 Dependence on feedback parameters

Finally, we use the CAMELS-SAM 1P set of simulations to test the effect of various feedback parameters on the topology of galaxy dis-

tributions. We have three parameters that are varied:  $A_{\text{SN1}}$ ,  $A_{\text{SN2}}$ , and  $A_{\text{AGN}}$ . For each parameter, there are two simulations (with different initial seeds) that use its maximum value and two that use its minimum value. All other parameters are kept at their fiducial values.

As before, for each simulation we select samples of star-forming and quiescent galaxies and compute their scaled Betti curves. We additionally average each pair of Betti curves to get mean Betti curves for the maximum and the minimum values of each feedback parameter.

In [Figure 7](#) we show how the Betti curves of star-forming and quiescent galaxies vary in response to these three parameters. The quiescent galaxies are much more sensitive to changes in these parameters than the star-forming galaxies. The strength of the AGN feedback has very little effect on the topology of these galaxy samples, while the supernova parameters have a very significant effect on the topology of the quiescent galaxies. Increasing the strength of the supernova feedback increases the number of  $H_1$  and  $H_2$  features at large scales and suppresses the peak at small scales. This suggests that these Betti curves should be able to differentiate different models of feedback.

## 7 SUMMARY AND FUTURE OUTLOOK

We used Betti curves from persistent homology to characterize the large-scale structure of simulated galaxies and DM haloes. To our knowledge, this is the first time such techniques from TDA have been applied to catalogs of both galaxies and haloes.

We showed that these topological summaries reveal differences in the large-scale structure of haloes and different galaxy populations. First, we found that DM haloes exhibit a nearly universal topology across a wide range of scales, after accounting for the effect of their number density. Even though haloes selected by mass cluster very differently, all haloes seem to trace the same topology. Galaxies, on the other hand, exhibit surprising differences on small scales. We found that a second physical scale shows up in the topology of galaxies that is not present in the haloes. We identify this additional structure present at small scales as coming from galaxies inside clusters. This is supported by the fact that this peak in the Betti curves is present only in the quiescent galaxies; the star-forming ones look very similar to the DM haloes. Further, by looking at parameter variations in the CAMELS-SAM simulations, we found that the topology of quiescent galaxies is especially sensitive to differences in the feedback model used. Based on these results, we argue that galaxies are topologically distinct from DM haloes and that topological summaries could provide very useful information in order to better constrain models of galaxy formation and evolution.

This paper also adds to the body of literature advocating for the use of summary statistics that probe higher-order aspects of clustering. Persistent homology provides a very natural way of quantifying the topology of large-scale structure in the universe, due to the wide range of physical scales present.

There are many future directions for this work. So far we have only looked at the Betti curves for the final  $z = 0$  snapshots of simulations. It would be very interesting to look at the redshift evolution of the Betti curves, and to construct lightcones to investigate the topology of galaxies in redshift space. Potentially, looking at the time evolution of the redshift-space topology of quiescent galaxies could help constrain when and how star formation shuts off inside clusters.

Additionally, there are many more simulated catalogs that this method could be applied to in order to check if these topological features are consistent across all models. Large hydrodynamic cos-

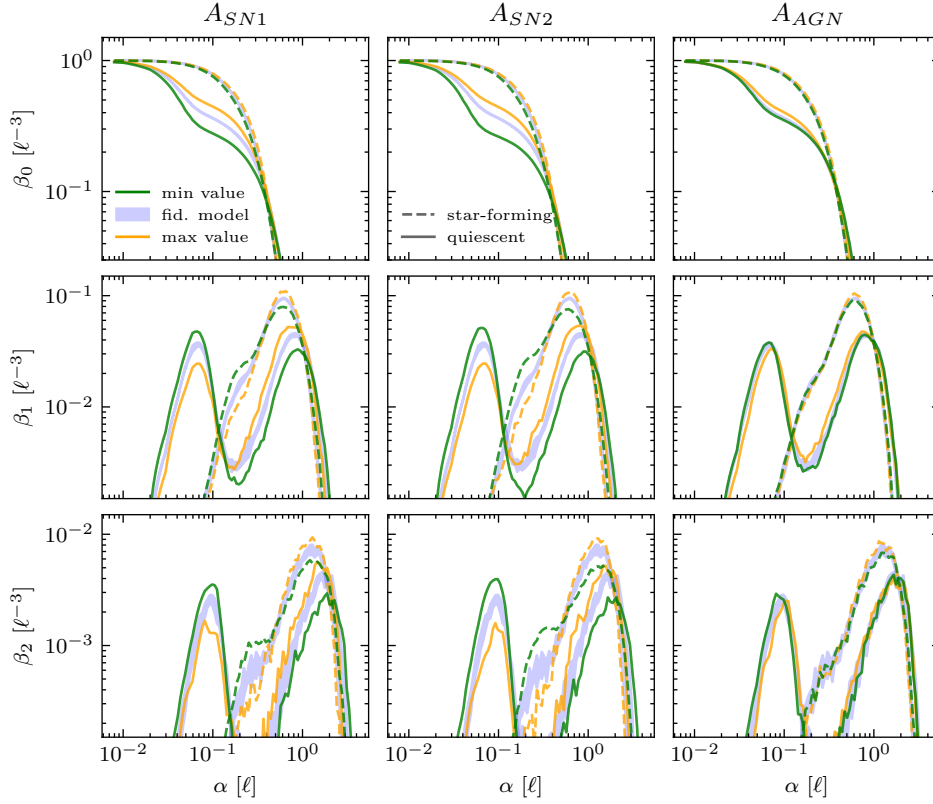


**Figure 7.** Betti curves for the star-forming and quiescent galaxies from the CAMELS-SAM 1P simulations. Each column shows how variations in the corresponding feedback parameter causes changes in the Betti curves. Here the solid/dashed lines represent the quiescent/star-forming galaxies, while orange/green represent the minimum/maximum value of the corresponding feedback parameter. The faint blue bands in between the lines show the  $2\sigma$  variation of the fiducial CAMELS-SAM model.

mological simulations are constantly improving (MillenniumTNG Pakmor et al. (2022), in particular, looks extremely promising) and we hope to fully utilize them to better understand the constraining power of these topological summaries. We are also interested in comparing alternatives to full hydrodynamic simulations, for example other semi-analytic models or halo occupation distribution models.

In the end, we hope to apply these techniques to observational data. We hypothesize that topological summaries, like the Betti curves used here, could provide useful observational constraints to compare to simulations of galaxy formation.

## ACKNOWLEDGEMENTS

We thank the TNG and CAMELS collaborations for publicly releasing their simulation data and example analysis scripts.

The analysis in this work was mainly carried out using Python. In addition to the previously cited software, the following packages were extremely useful: numpy (Harris et al. 2020), scipy (Virtanen et al. 2020), matplotlib (Hunter 2007), IPython (Perez & Granger 2007), h5py, and mpi4py (Dalcin & Fang 2021).

This work made use of the Illinois Campus Cluster, a computing resource that is operated by the Illinois Campus Cluster Program (ICCP) in conjunction with the National Center for Supercomputing Applications (NCSA) and which is supported by funds from the University of Illinois at Urbana-Champaign.

## DATA AVAILABILITY

All simulation data used in this work is publicly available. The analysis code has been posted on Github<sup>9</sup>. Any other data will be shared upon reasonable request to the corresponding author.

## REFERENCES

- Abazajian K., et al., 2019, [arXiv e-prints](#), p. arXiv:1907.04473
- Atienza N., Gonzalez-Díaz R., Soriano-Trigueros M., 2020, [Pattern Recognition](#), 107, 107509
- Banerjee A., Abel T., 2021, [MNRAS](#), 500, 5479
- Behroozi P. S., Wechsler R. H., Wu H.-Y., 2013a, [ApJ](#), 762, 109
- Behroozi P. S., Wechsler R. H., Wu H.-Y., Busha M. T., Klypin A. A., Primack J. R., 2013b, [ApJ](#), 763, 18
- Bermejo R., Wilding G., van de Weygaert R., Jones B. J. T., Vegter G., Efsthathiou K., 2022, [arXiv e-prints](#), p. arXiv:2206.14655
- Berry E., Chen Y.-C., Cisewski-Kehe J., Fasy B. T., 2020, [Journal of Applied and Computational Topology](#), 4, 211
- Biagetti M., Cole A., Shiu G., 2021, [J. Cosmology Astropart. Phys.](#), 2021, 061
- Biagetti M., Calles J., Castiblanco L., Cole A., Noreña J., 2022, [J. Cosmology Astropart. Phys.](#), 2022, 002
- Bond J. R., Kofman L., Pogossyan D., 1996, [Nature](#), 380, 603
- Bubenik P., 2012, [arXiv e-prints](#), p. arXiv:1207.6437
- Carlsson G., 2009, [Bulletin of the American Mathematical Society](#), 46, 255

<sup>9</sup> <https://github.com/ajouellette/galaxy-topology>



- Carlsson G., Zomorodian A., Collins A., Guibas L. J., 2005, *International Journal of Shape Modeling*, 11, 149
- Chazal F., Fasy B. T., Lecci F., Rinaldo A., Wasserman L., 2013, arXiv e-prints, p. [arXiv:1312.0308](https://arxiv.org/abs/1312.0308)
- Chisari N. E., et al., 2019, *The Open Journal of Astrophysics*, 2, 4
- Cisewski-Kehe J., Fasy B. T., Hellwing W., Lovell M. R., Drozda P., Wu M., 2022, *Phys. Rev. D*, 106, 023521
- Cole A., Biagetti M., Shiu G., 2020, arXiv e-prints, p. [arXiv:2012.03616](https://arxiv.org/abs/2012.03616)
- Coles P., Jones B., 1991, *MNRAS*, 248, 1
- Conroy C., et al., 2005, *ApJ*, 635, 990
- Coutinho B. C., Hong S., Albrecht K., Dey A., Barabási A.-L., Torrey P., Vogelsberger M., Hernquist L., 2016, arXiv e-prints, p. [arXiv:1604.03236](https://arxiv.org/abs/1604.03236)
- Crain R. A., et al., 2015, *MNRAS*, 450, 1937
- DESI Collaboration et al., 2016, arXiv e-prints, p. [arXiv:1611.00036](https://arxiv.org/abs/1611.00036)
- Dalcin L., Fang Y.-L. L., 2021, *Computing in Science & Engineering*, 23, 47
- Dlotko P., 2022, in , GUDHI User and Reference Manual, 3.6.0 edn, GUDHI Editorial Board, [https://gudhi.inria.fr/doc/3.6.0/group\\_persistence\\_representations.html](https://gudhi.inria.fr/doc/3.6.0/group_persistence_representations.html)
- Edelsbrunner H., Harer J. L., 2010, *Computational Topology: An Introduction*. American Mathematical Society
- Edelsbrunner H., Mücke E. P., 1994, *ACM Transactions on Graphics*, 13, 43
- Edelsbrunner H., Kirkpatrick D., Seidel R., 1983, *IEEE Transactions on Information Theory*, 29, 551
- Edelsbrunner Letscher Zomorodian 2002, *Discrete & Computational Geometry*, 28, 511
- Elbers W., van de Weygaert R., 2019, *MNRAS*, 486, 1523
- Elbers W., van de Weygaert R., 2023, *MNRAS*
- Ghrist R., 2007, *Bulletin of the American Mathematical Society*, 45, 61
- Gott J. Richard I. I. I., Melott A. L., Dickinson M., 1986, *ApJ*, 306, 341
- Gott J. Richard I. I. I., Weinberg D. H., Melott A. L., 1987, *ApJ*, 319, 1
- Gott J. Richard I. I. I., et al., 1989, *ApJ*, 340, 625
- Hamilton A. J. S., Gott J. Richard I. I. I., Weinberg D., 1986, *ApJ*, 309, 1
- Harris C. R., et al., 2020, *Nature*, 585, 357
- Hatcher A., 2001, *Algebraic Topology*. Cambridge University Press
- Heydenreich S., Brück B., Harnois-Déraps J., 2021, *A&A*, 648, A74
- Heydenreich S., Brück B., Burger P., Harnois-Déraps J., Unruh S., Castro T., Dolag K., Martinet N., 2022, *A&A*, 667, A125
- Hong S., Coutinho B. C., Dey A., Barabási A.-L., Vogelsberger M., Hernquist L., Gebhardt K., 2016, *MNRAS*, 459, 2690
- Humphrey A., et al., 2022, arXiv e-prints, p. [arXiv:2209.13074](https://arxiv.org/abs/2209.13074)
- Hunter J. D., 2007, *Computing in Science & Engineering*, 9, 90
- Ivezić Ž., et al., 2019, *ApJ*, 873, 111
- Kono K. T., Takeuchi T. T., Cooray S., Nishizawa A. J., Murakami K., 2020, arXiv e-prints, p. [arXiv:2006.02905](https://arxiv.org/abs/2006.02905)
- Landy S. D., Szalay A. S., 1993, *ApJ*, 412, 64
- Laureijs R., et al., 2011, arXiv e-prints, p. [arXiv:1110.3193](https://arxiv.org/abs/1110.3193)
- Leicht O., Uhlemann C., Villaescusa-Navarro F., Codis S., Hernquist L., Genel S., 2019, *MNRAS*, 484, 269
- Libeskind N. I., et al., 2018, *MNRAS*, 473, 1195
- Marinacci F., et al., 2018, *MNRAS*, 480, 5113
- Melott A. L., Weinberg D. H., Gott J. Richard I. I. I., 1988, *ApJ*, 328, 50
- Melott A. L., Cohen A. P., Hamilton A. J. S., Gott J. Richard I. I. I., Weinberg D. H., 1989, *ApJ*, 345, 618
- Murray S. G., 2018, *The Journal of Open Source Software*, 3, 850
- Naidoo K., Whiteway L., Massara E., Gualdi D., Lahav O., Viel M., Gil-Marín H., Font-Ribera A., 2020, *MNRAS*, 491, 1709
- Naiman J. P., et al., 2018, *MNRAS*, 477, 1206
- Nelson D., et al., 2015, *Astronomy and Computing*, 13, 12
- Nelson D., et al., 2018, *MNRAS*, 475, 624
- Nelson D., et al., 2019, *Computational Astrophysics and Cosmology*, 6, 2
- Pakmor R., et al., 2022, arXiv e-prints, p. [arXiv:2210.10060](https://arxiv.org/abs/2210.10060)
- Peebles P. J. E., 1980, *The Large-Scale Structure of the Universe*. Princeton University Press
- Peng Y.-j., et al., 2010, *ApJ*, 721, 193
- Perez F., Granger B. E., 2007, *Computing in Science & Engineering*, 9, 21
- Perez L. A., Malhotra S., Rhoads J. E., Tilvi V., 2021, *ApJ*, 906, 58
- Perez L. A., Genel S., Villaescusa-Navarro F., Somerville R. S., Gabrielpillai A., Anglés-Alcázar D., Wandelt B. D., Yung L. Y. A., 2022, arXiv e-prints, p. [arXiv:2204.02408](https://arxiv.org/abs/2204.02408)
- Pillepich A., et al., 2018, *MNRAS*, 473, 4077
- Pranav P., 2021, arXiv e-prints, p. [arXiv:2109.08721](https://arxiv.org/abs/2109.08721)
- Pranav P., Edelsbrunner H., van de Weygaert R., Vegter G., Kerber M., Jones B. J. T., Wintraecken M., 2017, *MNRAS*, 465, 4281
- Pranav P., et al., 2019, *MNRAS*, 485, 4167
- Robins V., 2002, in , *Morphology of Condensed Matter*. Springer Berlin Heidelberg, pp 261–274, doi:[10.1007/3-540-45782-8\\_11](https://doi.org/10.1007/3-540-45782-8_11)
- Robins V., 2006, *Phys. Rev. E*, 74, 061107
- Schaye J., et al., 2015, *MNRAS*, 446, 521
- Sinha M., Garrison L., Hearin A., Bradshaw C., Perez L. A., Hand N., Badger T. G., Beltz-Mohrmann G., 2021, manodeep/Corrfunc: Corrfunc-2.4.0, Zenodo, doi:[10.5281/zenodo.5541052](https://doi.org/10.5281/zenodo.5541052), <https://ui.adsabs.harvard.edu/abs/2021zndo...5541052S>
- Somerville R. S., Primack J. R., 1999, *MNRAS*, 310, 1087
- Somerville R. S., Hopkins P. F., Cox T. J., Robertson B. E., Hernquist L., 2008, *MNRAS*, 391, 481
- Somerville R. S., Popping G., Trager S. C., 2015, *MNRAS*, 453, 4337
- Sousbie T., 2011, *MNRAS*, 414, 350
- Springel V., White S. D. M., Tormen G., Kauffmann G., 2001, *MNRAS*, 328, 726
- Springel V., et al., 2018, *MNRAS*, 475, 676
- The GUDHI Project 2022, GUDHI User and Reference Manual, 3.6.0 edn. GUDHI Editorial Board, <https://gudhi.inria.fr/doc/3.6.0/>
- Thélie E., Aubert D., Gillet N., Ocvirk P., 2022, *A&A*, 658, A139
- Tsizh M., Tymchyshyn V., Vazza F., 2023, arXiv e-prints, p. [arXiv:2301.09411](https://arxiv.org/abs/2301.09411)
- Turner K., Mileiko Y., Mukherjee S., Harer J., 2014, *Discrete & Computational Geometry*, 52, 44
- Uhlemann C., Friedrich O., Villaescusa-Navarro F., Banerjee A., Codis S., 2020, *MNRAS*, 495, 4006
- Villaescusa-Navarro F., et al., 2022, arXiv e-prints, p. [arXiv:2201.01300](https://arxiv.org/abs/2201.01300)
- Virtanen P., et al., 2020, *Nature Methods*, 17, 261
- Vogelsberger M., et al., 2014, *Nature*, 509, 177
- Weinberg D. H., Gott J. Richard I. I. I., Melott A. L., 1987, *ApJ*, 321, 2
- Weinberger R., et al., 2017, *MNRAS*, 465, 3291
- Weinberger R., Springel V., Pakmor R., 2020, *ApJS*, 248, 32
- Wetzel A. R., Tinker J. L., Conroy C., van den Bosch F. C., 2013, *MNRAS*, 432, 336
- White S. D. M., 1979, *MNRAS*, 186, 145
- Xu X., Cisewski-Kehe J., Green S. B., Nagai D., 2019, *Astronomy and Computing*, 27, 34
- van Daalen M. P., Schaye J., Booth C. M., Dalla Vecchia C., 2011, *MNRAS*, 415, 3649
- van de Weygaert R., Bond J. R., 2008, in Plionis M., López-Cruz O., Hughes D., eds., Vol. 740, *A Pan-Chromatic View of Clusters of Galaxies and the Large-Scale Structure*. Springer Netherlands, pp 335–408, doi:[10.1007/978-1-4020-6941-3\\_10](https://doi.org/10.1007/978-1-4020-6941-3_10), <https://ui.adsabs.harvard.edu/abs/2008LNP...740..335V>
- van de Weygaert R., Vegter G., Platen E., Eldering B., Kruithof N., 2010, arXiv e-prints, p. [arXiv:1006.2765](https://arxiv.org/abs/1006.2765)
- van de Weygaert R., et al., 2011, in , Vol. 6970, *Lecture Notes in Computer Science*. Springer Berlin Heidelberg, pp 60–101, doi:[10.1007/978-3-642-25249-5\\_3](https://doi.org/10.1007/978-3-642-25249-5_3), <https://ui.adsabs.harvard.edu/abs/2011LNCS.6970...60V>

This paper has been typeset from a  $\text{\LaTeX}$  file prepared by the author.